

Elsevier Editorial System(tm) for Biomaterials
Manuscript Draft

Manuscript Number:

Title: Spherical bioactive glass particles and their interaction with human mesenchymal stem cells in vitro

Article Type: FLA Original Research

Section/Category: Biomaterials & Biocompatibility

Keywords: bioactive glass; sub-micron particles; stem cells; cytotoxicity; cellular uptake

Corresponding Author: Dr Julian R. Jones, PhD

Corresponding Author's Institution: Imperial College London

First Author: Sheyda Labbaf

Order of Authors: Sheyda Labbaf; Olga Tsigkou; Karin H Muller; Molly M Stevens; Alexandra E Porter; Julian R. Jones, PhD

Abstract: Sub-micron particles of bioactive glass (SMBGs) with composition 85 mol% SiO₂ and 15 mol% CaO were synthesised and characterised. Bioactivity was demonstrated by the formation of calcium apatite following 5 days immersion in simulated body fluid (SBF). The effect of a 24 h exposure of SMBGs (100 µgml⁻¹, 150 µgml⁻¹, 200 µgml⁻¹) to human mesenchymal stem cells (hMSCs) on cell viability, metabolic activity and proliferation was determined using the LIVE/DEAD, MTT, total DNA and LDH assays after 1, 4 and 7 days of culture. None of the SMBG concentrations caused significant cytotoxicity, except the highest doses of 150 and 200 µgml⁻¹ which significantly decreased hMSC metabolic activity after 7 days of culture. Cell proliferation decreased as SMBG concentration increased; however none of the SMBGs tested had a significant effect on DNA quantity compared to the control. Confocal microscopy confirmed cellular uptake and localisation of the SMBGs in the hMSC cytoskeleton. Transmission electron microscopy revealed that the SMBGs localised inside the cell cytoplasm and cell endosomes. These findings are important for assessing the toxicity of sub-micron particles that may either be used as injectables for bone regeneration or generated by wear or degradation of bioactive glass scaffolds.

AUTHOR DECLARATION TEMPLATE

We the undersigned declare that this manuscript is original, has not been published before and is not currently being considered for publication elsewhere.

We wish to confirm that there are no known conflicts of interest associated with this publication and there has been no significant financial support for this work that could have influenced its outcome.

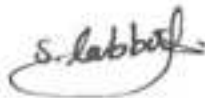
We confirm that the manuscript has been read and approved by all named authors and that there are no other persons who satisfied the criteria for authorship but are not listed. We further confirm that the order of authors listed in the manuscript has been approved by all of us.

We confirm that we have given due consideration to the protection of intellectual property associated with this work and that there are no impediments to publication, including the timing of publication, with respect to intellectual property. In so doing we confirm that we have followed the regulations of our institutions concerning intellectual property.

We understand that the Corresponding Author is the sole contact for the Editorial process (including Editorial Manager and direct communications with the office). He/she is responsible for communicating with the other authors about progress, submissions of revisions and final approval of proofs. We confirm that we have provided a current, correct email address which is accessible by the Corresponding Author and which has been configured to accept email from biomaterials@online.be.

Signed by all authors as follows:

Sheyda Labbaf



Dr Olga Tsigkou



Dr Karin Muller,

Karin Muller 18.06.'10

Professor Molly M. Stevens,



Dr Alexandra E. Porter,



Dr Julian R. Jones



Department of Materials
Imperial College London
South Kensington Campus
Exhibition Road
London SW7 2AZ
UK
Tel: +44 (0) 207 5946749
Fax: +44 (0) 20 7594 6757

julian.r.jones@imperial.ac.uk
www.imperial.ac.uk/materials

Dr Julian R. Jones
Senior Lecturer
PhD DIC MEng (Oxon) FIMMM

7/7/2010

Dear Professor Williams

We hope you will find our manuscript of interest. It describes the synthesis of new spherical bioactive glass sub-micron particles. We believe they are the smallest dispersed bioactive particles of proven bioactive composition that have been synthesised. The toxicity and uptake of the particles by stem cells is also reported for the first time. Properties of materials and cellular response to them can change when particles are small. For example small particles can be uptaken by cells where larger ones cannot. Cellular response to such particles is important because the particles could be used as injectable synthetic bone grafts and also because other implantable bioactive glasses may release small particles during degradation or when under load. When particles are uptaken by cells it is important to determine where they are localised in the cell and if they cause toxicity.

Best wishes

A handwritten signature in black ink, appearing to be 'Julian Jones', written over a horizontal line.

Dr Julian Jones
Imperial College London

Spherical bioactive glass particles and their interaction with human mesenchymal stem cells *in vitro*

Sheyda Labbaf¹, Olga Tsigkou¹, Karin H Müller^{1,3}, Molly M. Stevens^{1,2}, Alexandra E. Porter¹, Julian R. Jones*¹

¹Department of Materials, Imperial College London, South Kensington Campus, London, SW7 2AZ, UK

²Institute of Biomedical Engineering, Imperial College London, South Kensington Campus, London, SW7 2AZ, UK

³Multi-Imaging Centre, Department of Physiology, Development and Neuroscience, Cambridge University, Downing Street, Cambridge CB2 3DY, UK

*Corresponding author: julian.r.jones@imperial.ac.uk

Abstract

1 Sub-micron particles of bioactive glass (SMBGs) with composition 85 mol% SiO₂
2 and 15 mol% CaO were synthesised and characterised. Bioactivity was demonstrated
3 by the formation of calcium apatite following 5 days immersion in simulated body
4 fluid (SBF). The effect of a 24 h exposure of SMBGs (100 µgml⁻¹, 150 µgml⁻¹, 200
5 µgml⁻¹) to human mesenchymal stem cells (hMSCs) on cell viability, metabolic
6 activity and proliferation was determined using the LIVE/DEAD, MTT, total DNA
7 and LDH assays after 1, 4 and 7 days of culture. None of the SMBG concentrations
8 caused significant cytotoxicity, except the highest doses of 150 and 200 µgml⁻¹ which
9 significantly decreased hMSC metabolic activity after 7 days of culture. Cell
10 proliferation decreased as SMBG concentration increased; however none of the
11 SMBGs tested had a significant effect on DNA quantity compared to the control.
12 Confocal microscopy confirmed cellular uptake and localisation of the SMBGs in the
13 hMSC cytoskeleton. Transmission electron microscopy revealed that the SMBGs
14 localised inside the cell cytoplasm and cell endosomes. These findings are important
15 for assessing the toxicity of sub-micron particles that may either be used as injectables
16 for bone regeneration or generated by wear or degradation of bioactive glass
17 scaffolds.
18
19
20
21
22
23
24
25
26
27
28
29
30
31
32
33
34
35
36
37
38
39
40
41
42
43
44
45
46
47
48
49
50
51
52
53
54
55
56
57
58
59
60
61
62
63
64
65

1 Introduction

1
2
3
4 Bioactive glasses are promising materials for hard tissue regeneration because of their
5 distinctive properties of rapid bone bonding, controlled biodegradability and ability to
6 stimulate new bone growth [1]. Bone bonding arises due to the formation of an apatite
7 layer on the glass surface following contact with body fluid [2] and osteogenesis is
8 thought to be stimulated by the release of ions from the glass which triggers cell
9 activity [1]. Current commercially available BG particles include NovaBone
10 (NovaBone Products LLC, Alachua, Florida) which is used in a wide range of dental
11 and orthopaedic applications. Novabone[®] has the composition known as 45S5
12 Bioglass[®] (46.1 mol% SiO₂, 26.9 mol% CaO, 24.4 mol% Na₂O and 2.5 mol% P₂O₅).
13
14
15
16
17
18
19
20

21 The particles are in the micrometer size-range (90-710µm) and are irregular in size
22 and shape. Sub-micron bioactive glass particles (SMBG), are an attractive alternative
23 to bioactive glass microparticles for hard tissue regeneration as their small size and
24 higher specific surface area makes them ideal for injection into the bone defects or
25 incorporation within a polymeric matrix to synthesise porous composite scaffolds.
26
27
28
29

30 Sol-gel derived bioactive glasses tend to contain fewer components than the melt-
31 derived glasses and can exhibit enhanced bioactivity and resorbability due to their
32 increased surface area, provided by the nanoporosity inherent to the sol-gel process.
33 Higher surface area significantly enhances their solubility [3]. Recently, Hong *et al*
34 [4] used the sol-gel process to produce SiO₂-CaO-P₂O₅ ternary glass-ceramic
35 nanoparticles (20 nm). The small size of the particles is likely to be responsible for the
36 crystallisation during thermal stabilisation because driving force for nucleation of
37 crystals increases with specific surface area. The phosphate in the ternary system is
38 not an essential component for bioactivity as the low quantities of phosphate in sol-
39 gel bioactive glass forms orthophosphate [5], which is loosely bound to the glass
40 network and lost rapidly in dissolution, and, the surface will adsorb phosphate ions
41 from the body fluid [6]. Phosphate-free glasses in the binary system SiO₂-CaO have
42 been shown to exhibit both *in vitro* and *in vivo* bioactivity [7, 8]. Martines *et al* [9]
43 studied the compositional range of 50-90 mol% SiO₂ in sol-gel glasses to investigate
44 the compositional limits of bioactivity in SBF. Their results demonstrated that all
45 glasses were bioactive in that they formed an apatite layer in SBF such that with
46 increased SiO₂ in the composition the rate of formation of apatite decreased [9]. Sol-
47
48
49
50
51
52
53
54
55
56
57
58
59
60
61
62
63
64
65

1 gel glasses can be bioactive at high silica contents not only because they have high
2 specific surface area but also because they contain a broad distribution of network
3 connectivity (average number of bridging oxygen bonds per silicon atom). This is due
4 to hydrogen acting as an additional network modifier, disrupting the silica network,
5 creating a high concentration of Si-OH groups [10]. This increases the rate of
6 dissolution and provides sites for apatite nucleation. An aim of this work was to
7 synthesise binary SMBGs in the sub-micron range and to maintain their amorphous
8 structure for controlled bioactivity.

9 Previously particles of the 100S (100 mol% SiO₂) composition have been produced
10 by the Stöber process [11]. This process was modified by Zhao *et al* [12] to produce
11 particles of mesoporous silica spheres from silica/hyperbranched polyester
12 nanocomposite via the sol-gel method by using BoltornTM (H2O) polymer as a
13 templating agent. This hyperbranched polyester has a 3D architecture and 16 hydroxy
14 end-groups per molecule [13]. The use of BoltornTM polymer into the synthesis route
15 enhances the dispersability and the formation of spherical particles.

16 Despite the great potential of bioactive glasses as porous scaffolds for bone
17 regeneration [14], concerns have arisen about their long term fate in the body as wear
18 particles of nano- or micrometer size may be generated after implantation, which
19 could potentially cause adverse reactions with surrounding cells. These cellular
20 reactions may be due to particular characteristics of particles including their size, high
21 surface area to volume ratio or their surface chemistry. To date, very little is known
22 about the interaction of SMBG with the body with regards to their toxicity. It is
23 hypothesised that SMBGs enter cells by endocytosis, localise inside endosomes and
24 dissolve resulting in raised localised soluble silica and calcium concentrations. A
25 localised increase in intracellular silica or calcium could cause a marked effect on cell
26 metabolism [15] or inflammatory response [16]. As particles dissolve intracellularly,
27 they may also break up into finer particles which are able to escape the endosomal
28 pathway and enter the cell cytoplasm or even the nucleus causing raised levels of
29 cytotoxicity. This process has been demonstrated previously with HA particles
30 exposed to human macrophage cells [17] and will therefore be investigated here for
31 SMBGs.

32 Imaging the intracellular fate of SMBGs can help to elucidate how they enter the
33 cells, their biodistribution, retention, degradation inside the cell and whether, as a
34 result, they affect any cellular function [18]. Previously silica particles have been
35
36
37
38
39
40
41
42
43
44
45
46
47
48
49
50
51
52
53
54
55
56
57
58
59
60
61
62
63
64
65

1
2
3
4
5
6
7
8
9
10
11
12
13
14
15
16
17
18
19
20
21
22
23
24
25
26
27
28
29
30
31
32
33
34
35
36
37
38
39
40
41
42
43
44
45
46
47
48
49
50
51
52
53
54
55
56
57
58
59
60
61
62
63
64
65

imaged inside cells with confocal microscopy, by fluorescently labelling the particles [19, 20]. However, labelling particles may modify their interaction with the cell. Transmission electron microscopy (TEM) has also been used to image, at high resolution the intracellular distribution and stability of HA and silica nanoparticles [17, 20, 21]. However, visualising the subcellular distribution of SMBG in the TEM is challenging as it is difficult to prepare sections across the SMBG-cell interface due to differences in the hardness of the two materials. In this study we demonstrate that it is possible to image unlabelled SMBGs in 3D using confocal microscopy in reflectance mode and also to prepare sections of cells, which have internalised SMBGs via ultramicrotomy for analysis by TEM imaging.

Bone-marrow derived human mesenchymal stem cells (hMSC) are an attractive cell source for tissue-engineering applications because of their relative ease of isolation and expansion from adult bone marrow aspirates and their potential for pluripotent differentiation into mesenchymal tissues [22]. Previous studies have reported that cells derived from bone marrow can be stimulated towards osteogenesis when in contact with bioactive glasses [23]. hMSCs are also believed to egress from bone marrow and migrate towards the site of bone injury, home there and differentiate to promote repair [24]. Also, hMSCs are precursors to osteoblasts, hence the effect of particles on their behaviour is critical. For these reasons, hMSCs are a relevant cell type to use to test the biocompatibility of SMBGs.

The overall aim of this study was to synthesise and characterise binary SMBGs and to investigate their effect on cellular behaviour. The effect of these particles on cell viability, metabolic activity and proliferation of hMSC was then studied using LIVE/DEAD, MTT, total DNA and LDH assays. Finally, TEM and 3-D confocal microscopy were applied to assess the distribution of SMBGs inside hMSC and whether they dissolve intracellularly.

2 Material and methods

Processing of BG sub-micron particles

The methodology used by Zhao *et al* [12] for synthesis of 100S (100 mol% SiO₂) was modified to obtain 85S15C (85 mol% SiO₂ and 15 mol% CaO) SMBG, produced using sol-gel process, that involves the hydrolysis of tetraethyl orthosilicate (TEOS, Si(OCH₂CH₃)₄), and condensation of resulting species. The effect of Boltorn™

1 polymer (H20 hyperbranched polyester average molecular weight of 1735 g mol⁻¹,
2 Pertorp AB, UK, which will be referred to as B-polymer) content on particle size and
3 dispersability was then investigated by using molar ratio of templating polymer to
4 TEOS of 1 : 1, 1 : 5.7, 1 : 2.8 and 1 : 2.2 of B-polymer was mixed with 50 ml of 1,4-
5 dioxane under stirring at a temperature of 90 °C. Then 2.6 ml of H₂O and 9.7 ml of
6 NH₃.H₂O were added to the mixture followed by the addition of 2.8 ml of TEOS
7 dropwise at 50 °C. The mixture was gently stirred for 1 h for complete hydrolysis;
8 after which 1.26 g of Ca(NO₃)₂.4H₂O was added and left to mix for 24 h. A reference
9 sample with no polymer (PO) was also synthesised. The resulting colloidal suspension
10 was then centrifuged to obtain a white solid suspension. The deposited solid was
11 vacuum dried to remove excess water from the solid particles, producing a white
12 powder. To remove the organic phase and the nitrate from the network, the resulting
13 powders were calcined in air. A molar ratio of templating polymer to TEOS of 1 : 2.8
14 was the only concentration that formed dispersed spherical SMBGs. The effect of
15 calcination temperature on the structure of SMBGs was investigated at 680, 700 and
16 800 °C.
17
18
19
20
21
22
23
24
25
26
27
28
29
30

31 *Acid digestion compositional analysis*

32 This method was applied to measure the composition of SMBGs. 0.1 g of finely
33 ground glass was mixed carefully with 0.5 g of anhydrous lithium metaborate in a
34 clean dry platinum crucible using a glass rod. The mixture was fused for 1 h at 1400
35 °C and then left to cool. The crucible was then immersed in 80 ml of 10 vol% Nitric
36 acid to completely dissolve the flux and then transferred to a 100 ml polypropylene
37 volumetric flask and made up to the mark. A series of dissolution studies were carried
38 out to measure the ion concentration using inductively coupled plasma optical
39 emission spectroscopy (ICP-OES, Thermo Scientific Icap 6000series).
40
41
42
43
44
45
46
47
48

49 *Particle Characterisation*

50 X-ray Diffraction (XRD) spectra were collected on a Philips PW1700 series
51 automated powder diffractometer using Cu K α radiation at 40KV / 40mA. Data was
52 collected between 5-80° 2 θ with a step of 0.04° 2 θ and a dwell time of 1.5 seconds to
53 identify any crystallisation of the particles.
54
55
56
57
58
59
60
61
62
63
64
65

1
2 In order to confirm the removal of the organic component from the SMBGs, Fourier
3 transform infrared (FTIR) spectra were collected on the PerkinElmer Spectrum™ 100
4 FT-IR spectrometer, in the range of 600-2200 cm⁻¹.

5 Nitrogen sorption (Autosorb AS6, QuantaChrome) was performed to measure the
6 SMBG porosity by applying the BJH method [25] to the N₂ desorption branches of
7 the isotherms. B.E.T. analysis was used to determine the specific surface area of the
8 BNP [26]. The samples were prepared by degassing at room temperature overnight.
9
10
11
12

13 *Bioactivity*

14 To test the bioactivity of SMBGs, simulated body fluid (SBF) solution was prepared
15 following the procedure proposed by Kukubo *et al* [27]. 0.01 g SMBGs with 85S15C
16 composition, sintered at 680 °C, were immersed in 40ml of SBF at 37 °C at 175 rpm
17 for 48, 120 and 168 h. At the end of each time-point, the SMBG were dispersed in
18 SBF by ultrasonication, before being collected on 300 mesh lacey carbon film TEM
19 grids [28, 29].
20
21
22
23
24
25
26
27

28 *hMSC cell culture*

29 hMSCs were purchased from Lonza (Lonza, UK) and maintained in low glucose,
30 phenol red free, Dulbecco's Modified Eagle Medium (DMEM) supplemented with
31 10% (v/v) batch tested Fetal Bovine Serum (FBS), 50 U/ml penicillin and 50 µg/ml
32 streptomycin, 1% (v/v) L-glutamine (all from Invitrogen, UK) (which will be referred
33 to as complete medium).
34
35
36
37
38
39
40
41

42 hMSCs were seeded at a density of 10,000 cells/cm² and cultured with complete
43 medium containing SMBGs at concentrations of 0, 100, 150 and 200 µgml⁻¹. The
44 SMBG concentration was determined by drying to constant weight, then heat-
45 sterilised at 120 °C for 2 h, followed by UV sterilisation. The solution containing the
46 SMBGs was ultrasonicated to ensure an even suspension prior to adding to cells.
47 hMSCs were exposed to a pulse of SMBG for 24 h followed by chase periods of 1, 4
48 and 7 days. In accordance with previous studies [19, 30] a pulse of 24 h was chosen as
49 it has been demonstrated that hMSCs already internalise NPs by this time point. The
50 pulse-chase experiment was performed by removing the culture medium containing
51 the SMBGs after 24 h, washing the cells with PBS and adding fresh complete medium
52 to the cells. The viability of hMSCs was assessed using the LIVE-DEAD assay
53
54
55
56
57
58
59
60
61
62
63
64
65

1 (Molecular Probes, UK), MTT 3-(4,5-Dimethylthiazol-2-yl)-2,5-diphenyltetrazolium
2 bromide (Sigma), total DNA measurements and Lactate dehydrogenase (LDH)
3 Cytotox-oneTM assay (Promega, UK).
4
5
6

7 The LIVE/DEAD assay was performed according to the manufacturer's instructions to
8 examine SMBG cytotoxicity after 24 h. The assay utilises two fluorescent dyes to
9 label live and dead cells. The cytoplasm of live cells was stained with 2 µM calcein
10 (green) and the nucleus of dead cells stained with 4 µM EthD-1 (red). Stained cells
11 were viewed using the Olympus BX-URA2 fluorescence microscope. Images were
12 captured within 15 min of labelling using a Zeiss Axiocam digital camera and
13 analysed using KS-300 software (Imaging Associates).
14
15
16
17
18
19
20

21 Cell metabolic activity and consequently cell viability and proliferation over time was
22 assessed using the MTT assay. At the end of each time point, 20 µl of 5 mg/ml of
23 MTT solution were added to each well and incubated for 2 h at 37 °C. Sample
24 solutions were then removed and 200 µl of dimethyl sulfoxide was added to each
25 well. Plates were then incubated for 5 min to dissolve the crystals. Absorbance was
26 measured at 490 nm using the microplate spectrophotometer Anthos 2020 (Anthos
27 Biotech, Salzburg, Austria). The results represent the mean values ± standard
28 deviation (SD) of two individual experiments each performed in quadruplicate.
29
30
31
32
33
34
35
36

37 The effects of three different concentrations of SMBG on hMSC proliferation was
38 also assessed by measuring total cellular DNA in culture after 1, 4 and 7 days.
39 Medium was removed and extra pure water was added to each well followed by at
40 least three freeze-thaw cycles. 50 µl of the cell lysate and bis-Benzamid 33258
41 (Hoechst stain) (Sigma) in TNE buffer (10 Mm Tris, 1 mM EDTA, 2 M NaCl, pH
42 7.4) were transferred to a new 96 well plate. A standard curve was constructed using
43 calf thymus DNA (Sigma) to determine the DNA concentration. Fluorescence was
44 measured on a fluorescence plate reader (SpectraMAX GemimXS plate reader) at an
45 excitation/emission wavelength of 360/460 nm. The results represent the mean values
46 ± SD of two individual experiments each in quadruplicate.
47
48
49
50
51
52
53
54
55
56

57 The CytoTox-ONETM (Promega, UK) assay which assess' the cell membrane integrity
58 by measuring the leakage of lactate dehydrogenase (LDH) from cells, was used to
59
60
61
62
63
64
65

1 calculate the percent live and dead cells following exposure. To perform the assay,
2 LDH in the supernatant and in the adhered cells was measured separately. 50 µl of
3 centrifuged supernatant was added to 50 µl of reconstituted substrate mix and was
4 incubated at room temperature, protected from light, for 30 min. Adherent cells were
5 then lysed by adding 100 µl 0.9% Triton-X100 and incubated for 15 min at 37 °C.
6 Following incubation, 50 µl of the cell lysate was then added to 50 µl of LDH assay
7 mixture in a 96 well plate. Absorbance was measured at 490 nm with a reference
8 wavelength of 620 (Anthos 2020 Biotech, Salzburg, Austria). The total number of
9 viable cells is directly proportional to the LDH in the adherent cell lysates, whereas
10 the total number of dead cells is directly proportional to the LDH in the cell
11 supernatant according to the manufacturer's instructions .

12 Live cell percent is normalised to the total number of live cells of the control at day 1.

13 For 3D confocal microscopy imaging, the hMSCs were grown on chamber slides
14 (LabTek, UK) and exposed to SMBGs at a concentration of 100 µg/ml for 24 h. They
15 were then fixed in 4% (w/v) paraformaldehyde in PBS, with 1% sucrose at 37 °C for
16 20 min, washed with PBS and permeabilized with buffered 0.5% Triton X-100 (10.3g
17 sucrose, 0.292 g NaCl, 0.06 g MgCl₂, 0.476 g 4-(2-hydroxyethyl)-1-piperazine-
18 ethanesulphonic acid (HEPES), in 100 ml water (pH 7.2) at 4 °C for 5 min. The cells
19 were subsequently incubated for 1 h with Alexa 568-conjugated phalloidin (1:100,
20 Molecular Probes, UK). Background labelling was minimised by washing with 0.5%
21 Tween 20/PBS. Samples were mounted in Vectashield with DAPI (Vector
22 Laboratories, UK), and viewed with a Leica SP5 MP inverted (SAFB 408) confocal
23 microscope. The SMBGs were imaged in reflectance mode from the internalised
24 particles. Z-plane stacks were taken to generate 3-D reconstructions.

25 *Transmission electron microscopy (TEM)*

26 SMBGs were dispersed in ethanol and then collected on 300 mesh copper TEM grids,
27 coated with lacey carbon film. In order to quantify particle size, the diameter of
28 individual particles (n=149) was measured from TEM micrographs in Image J
29 software. The formation of the apatite layer on the surface of the particles was
30 characterised by TEM, selected electron diffraction (SAED) and energy-dispersive X-
31 ray spectroscopy (EDX). Images were taken after short exposure times to the electron
32 beam to ensure that no beam damage was induced to the particles during analysis.

1 For TEM analysis of cells, the cells were treated with 100 µg/ml of SMBGs for 24 h.
2 Following exposure, the cell monolayers were washed with 0.9% saline and fixed
3 with 4% glutaraldehyde in PIPES buffer (0.1 M, pH 7.2) for 1 h at 4 °C. The fixative
4 was then removed and samples were washed with saline to remove all unbound
5 glutaraldehyde. Scraped cells were then centrifuged into pellets and washed in saline.
6 This was followed by incubation in a solution of 1% osmium tetroxide containing
7 1.5% potassium ferricyanide and 2 mmol/L calcium chloride in 0.1 m PIPES buffer at
8 pH 7.4 for 1 h at room temperature. The cells were then washed 6 times in DIW and
9 dehydrated with graded solutions of ethanol (70, 95, and 100%) for 5 min in each
10 solution. Samples were then embedded in Quetol resin (Agar Scientific, UK) under
11 vacuum for 3 days and cured in fresh resin for 24 h at 60 °C. Thin sections (60–90
12 nm) were cut using a 35° diamond knife on a Leica Ultracut UCT ultramicrotome and
13 collected immediately onto bare 300 mesh copper grids and dried to eliminate any
14 possibility that the SMBGs dissolved in the water bath of the diamond knife. To
15 improve contrast from cell organelles, selected TEM sections were post-stained with
16 saturated methanolic uranyl acetate and lead citrate using a drop-to-drop method.
17 TEM imaging and EDX were performed on JEOL-2000FX and a 2010 FX II electron
18 microscopes, with an operating voltage of 120kV and a 10 µm objective aperture to
19 increase mass-thickness contrast and reduce knock-on damage to the SMBGs.
20 Multiple areas from 2 samples were observed in the TEM.
21
22
23
24
25
26
27
28
29
30
31
32
33
34
35
36
37

38 *Statistical analysis*

39 Statistical analysis was performed using the Sigma Stat software using the Student's t-
40 test. P-values of <0.05 were considered as statistically significant.
41
42
43
44

45 **3 Results**

46 **3.1 Characterisation of Nanoparticles**

47 Compositional analysis (ICP-OES) found the SMBG composition to be 85 mol%
48 SiO₂ and 15 mol% CaO (86.022 mol% SiO₂ and 13.98 mol% CaO, ±0.34). The XRD
49 spectra in Fig. 1 show that the SMBGs were amorphous when sintered at 680 and 700
50 °C (Fig. 1), but when sintered at 800 °C a peak at a 2θ value of 30° was observed that
51 corresponded to the wollastonite (β-CaSiO₃) phase [31] . Hence, an ideal sintering
52 temperature for the SMBGs is in the range 680<T<800 °C in order to retain the
53
54
55
56
57
58
59
60
61
62
63
64
65

1 particles in the amorphous state. For this study a sintering temperature of 680 °C was
2 chosen for further investigation.

3 The H2O B-polymer was mixed with the TEOS during the sol-gel process so that it
4 could act as a template to prevent agglomeration and further condensation of the
5 SMBGs. This created a composite (SMBG-H2O) which was calcined to remove the
6 polymer and reduce the silanol groups from the glass surface and nitrate by-products
7 from the glass network. Supplementary Fig. 1 shows FTIR spectra before and after
8 calcinations at 680 °C. A vibration band at around 1650 cm⁻¹ in the uncalcined
9 material corresponds to an ester group [12] and represents the organic phase. The
10 absorption band at 1020 cm⁻¹ corresponds to the mode of the Si-O-Si asymmetric
11 bond stretching vibration representing the silica network of the SMBGs. The band at
12 970 cm⁻¹ for the non-bridging oxygen vibration was present before calcination
13 (SMBG-H2O) but not after, suggesting the formation of more bridging Si-O-Si bonds
14 (increase in network connectivity) at the expense of Si-OH bonds during calcination.
15

16 An optimised SMBG synthesised using a molar ratio of templating polymer to TEOS
17 of 1:2.8 polymer is presented in Fig. 2a, where particles were spherical, with an
18 average diameter, measured using TEM, of 250 nm (±75nm, n=149) and modal
19 diameter of 175 nm, measured using dynamic light scattering (data not shown). EDX
20 analysis (Fig. 2b) confirms Si and Ca content in the SMBGs.
21
22
23
24
25

26 Nitrogen adsorption/desorption isotherms for SMBGs (supplementary Fig. 2) were
27 type II isotherms which indicated that the material has high affinity for nitrogen and
28 could either be non-porous or have a microporous (pores <2nm) structure [32]. The
29 mean BET surface area was 28 m²g⁻¹. It is possible that the surface area results were
30 also influenced by agglomeration between some of the particles (Fig. 2a) which
31 makes a large part of the surface of the particles inaccessible to N₂ molecules.
32
33
34
35

36 **3.2 Bioactivity testing**

37 TEM, EDX and SAED studies were performed to determine whether apatite had
38 formed on the surface of SMBGs. After 48 h immersion in SBF, the outer shell of the
39 SMBGs had reduced contrast with several fine, dense particulates surrounding them,
40 indicating dissolution (Fig. 3a). Fig. 3b illustrates that deposits had nucleated on the
41 surface of clusters of the particles within 48 h of immersion. Also, changes in
42 morphology around and on the surface of these particles can be seen (Fig. 3b). The
43
44
45
46
47
48
49
50
51
52
53
54
55
56
57
58
59
60
61
62
63
64
65

1 loss of mass-thickness contrast in the regions around the outer shell of the particles
2 was not caused by electron beam damage as adjacent regions of apatite did not display
3 a similar loss of contrast after irradiation with the electron beam. After 120 h
4 immersion (Fig. 3c) the nucleated deposits on the surface of the SMBG were
5 widespread and the particles had noticeably decreased in size. Fig. 3c shows
6 crystalline spots in SAED pattern from these deposits that are consistent with the
7 known hexagonal form of crystalline hydroxyapatite (HA) that has lattice parameters
8 $a = b = 9.4104 \text{ \AA}$, $c = 6.874760 \text{ \AA}$. EDX spectra (Fig. 3d) showed that the deposits
9 were calcium and phosphorus rich, which further confirmed the formation of HA.
10
11
12
13
14
15
16
17

18 **3.3 Cell viability**

19 The LIVE/DEAD cytotoxicity assay (supplementary Fig. 3) showed a high number of
20 live cells following exposure to 100 and 200 μgml^{-1} of SMBG after 24 h with few
21 dead cells. The LDH assay (Fig 4a) also demonstrated that none of the SMBG
22 concentrations tested were cytotoxic after 1, 4 and 7 days. The %LDH release in
23 viable cells decreased at day 4, but increased at day 7. This was consistent with the
24 increase in %LDH of dead cells that were seen to be highest in day 4 and decreased in
25 day 7. Also, at day 7 the %LDH is highest compared to day 1 and 4. Exposure to
26 SMBGs caused a dose and time dependent decrease in metabolic activity with the
27 MTT assay (Fig. 4b). A significant decrease in metabolic activity was only found
28 after 7 days in culture with 150 and 200 μgml^{-1} of SMBGs ($p < 0.05$). Total DNA
29 measurements (Fig 4c) demonstrated that cell proliferation increased in a dose-
30 dependent manner, with increasing SMBG concentration the cell proliferation
31 decreased, however none of the SMBG concentrations tested had a significant effect
32 on DNA quantity compared to the control cells.
33
34
35
36
37
38
39
40
41
42
43
44
45
46

47 **3.4 SMBG uptake by hMSCs**

48 To monitor the cellular uptake of the SMBGs, hMSCs were exposed to 100 μgml^{-1} of
49 SMBGs in medium for 24 h. Traditional 2D bright field TEM images and 3D
50 confocal microscopy reconstructions were compared to determine whether the
51 SMBGs were taken up by hMSCs. The light reflectance property of these SMBGs
52 enabled their visualisation inside the hMSCs using confocal microscopy without the
53 need of fluorochrome tag (Fig. 5). Optical sections were taken at intervals of 2 μm
54 along the z axis and reconstructed in 3D images to reveal randomly distributed
55
56
57
58
59
60
61
62
63
64
65

1 SMBGs spread between the actin microfilaments (Fig 5 b, c, d) of the hMSCs. The
2 supplementary movie shows a rotating 3D reconstruction of particles inside the cells.
3 These dense particles were not seen in the control cells (Fig. 5a). In TEM
4 micrographs, particles were internalised by cells (Fig. 6b). Again, none were observed
5 in controls (Fig. 6a). In post-stained sections, clusters of SMBGs were encapsulated
6 inside membrane-bound endosomes (Fig 6c, region i) and also inside the cell
7 cytoplasm (Fig. 6c, region ii). In some regions inside the cell there was a reduction in
8 mass-thickness contrast from the centre of the SMBGs suggesting that the particles
9 had partially dissolved and begun to hollow out (Fig. 7a, region iii). EDX of the
10 particle in Fig. 7a (region iii), confirmed the presence of Ca and Si in the particles
11 (Fig. 7b). No Si was detected away from the particle. The size of the particles also
12 appeared decreased inside the cells as a function of time in culture, providing further
13 possible evidence for SMBG dissolution (Fig. 6c, region ii). Some regions adjacent to
14 the endosomal membrane (Fig. 7a, region iv) were rich in calcium only and lacked an
15 observable silicon peak (Fig. 7c).

29 4 Discussion

30 85S15C SMBGs with a mean particle size of 250 nm (± 75 nm, n=149) were
31 successfully synthesised using the sol-gel process. The sol-gel process is a versatile
32 process whereby the growth mechanism, size and number of the nanoparticles in a
33 solution is mainly influenced by the rate of hydrolysis and condensation [33]. By
34 controlling the two reactions during the processing, the structure of final material can
35 be manipulated. For the synthesis of SMBGs, an ammonia catalyst was used to favour
36 the formation of spherical particles and to gain control of morphology and size by
37 controlling the rate of the condensation reaction. During the initial mixing stage of
38 sol-gel process, many of the functional OH groups at the surface of the polymer bond
39 to the surface of the hydrolysed silica particles. The remaining Si-OH groups undergo
40 further condensation and result in formation of more –Si-O-Si– bonds. The
41 mechanism for incorporation of calcium into the glass network as network modifier,
42 when using calcium nitrate precursor, has only recently been understood. The calcium
43 nitrate remains in the pore liquor (by product of the condensation reaction and excess
44 water from the hydrolysis) until drying is carried out. The calcium nitrate deposits
45 onto silica particle surfaces during drying and calcium only enters the glass network,
46 by diffusion, when the temperature 450 °C is reached during calcination [10]. Using

1 this method, it was not possible to synthesise spherical SMBGs with higher calcium
2 content. This is likely to be due to the calcium needing to diffuse into the particles
3 from their surface. The coating of the particles with B-polymer prior to addition of
4 calcium nitrate may limit the deposition of calcium nitrate onto the particles during
5 drying and therefore limit the diffusion of calcium into the particles. Hence, it is
6 challenging to incorporate Ca into the network and the current processing route limits
7 CaO content to 15 mol%.

8
9
10
11
12
13
14 Based on the XRD results, a sintering temperature of 680 °C was chosen for further
15 investigation for several different reasons: 1. A temperature greater than 450 °C is
16 needed for calcium to be incorporated into the silica network [34], 2. Above 500 °C
17 the organic phase is removed, 3. A temperature above 600 °C is needed to remove
18 residual nitrate and silanol groups and 4. Above 800 °C the glass begins to crystallise
19 (Fig. 1). Therefore, a temperature of 680 °C was chosen as it is believed that the
20 maximum bioactivity would be achieved at a minimum stabilisation temperature [14,
21 35], where the dissolution rate would be the most rapid (lowest network connectivity
22 and highest Si-OH group content).

23
24
25
26
27
28
29
30
31
32
33 The surface area of sol-gel derived sub-micron SMBG ($28 \text{ m}^2\text{g}^{-1}$) is much higher than
34 that of commercially available melt-derived microparticles ($2.7 \text{ m}^2\text{g}^{-1}$) [36]. The
35 reason for the non-porous nature of these sol-gel derived SMBG obtained in this
36 study, compared to conventional sol-gel particles, which have a surface area greater
37 than $100 \text{ m}^2\text{g}^{-1}$ [36], is that conventional sol-gel particles are made using acid
38 catalysed hydrolysis. During the acid-catalysed sol-gel process the nanoparticles in
39 the sol assemble during the condensation reaction and form a structure composed of
40 many sub-units (nanoparticles) that subsequently fuse together [10]. As a result, they
41 tend to leave interstitial spaces between the nanoparticles which become nanopores.
42 For the production of SMBG the condensation reaction is controlled by using base
43 catalysts that prevents the nanoparticles from fusing together, leaving individual
44 dense particles [33].

45
46
47
48
49
50
51
52
53
54
55
56
57
58
59
60
61
62
63
64
65
66
67
68
69
70
71
72
73
74
75
76
77
78
79
80
81
82
83
84
85
86
87
88
89
90
91
92
93
94
95
96
97
98
99
100
101
102
103
104
105
106
107
108
109
110
111
112
113
114
115
116
117
118
119
120
121
122
123
124
125
126
127
128
129
130
131
132
133
134
135
136
137
138
139
140
141
142
143
144
145
146
147
148
149
150
151
152
153
154
155
156
157
158
159
160
161
162
163
164
165
166
167
168
169
170
171
172
173
174
175
176
177
178
179
180
181
182
183
184
185
186
187
188
189
190
191
192
193
194
195
196
197
198
199
200
201
202
203
204
205
206
207
208
209
210
211
212
213
214
215
216
217
218
219
220
221
222
223
224
225
226
227
228
229
230
231
232
233
234
235
236
237
238
239
240
241
242
243
244
245
246
247
248
249
250
251
252
253
254
255
256
257
258
259
260
261
262
263
264
265
266
267
268
269
270
271
272
273
274
275
276
277
278
279
280
281
282
283
284
285
286
287
288
289
290
291
292
293
294
295
296
297
298
299
300
301
302
303
304
305
306
307
308
309
310
311
312
313
314
315
316
317
318
319
320
321
322
323
324
325
326
327
328
329
330
331
332
333
334
335
336
337
338
339
340
341
342
343
344
345
346
347
348
349
350
351
352
353
354
355
356
357
358
359
360
361
362
363
364
365
366
367
368
369
370
371
372
373
374
375
376
377
378
379
380
381
382
383
384
385
386
387
388
389
390
391
392
393
394
395
396
397
398
399
400
401
402
403
404
405
406
407
408
409
410
411
412
413
414
415
416
417
418
419
420
421
422
423
424
425
426
427
428
429
430
431
432
433
434
435
436
437
438
439
440
441
442
443
444
445
446
447
448
449
450
451
452
453
454
455
456
457
458
459
460
461
462
463
464
465
466
467
468
469
470
471
472
473
474
475
476
477
478
479
480
481
482
483
484
485
486
487
488
489
490
491
492
493
494
495
496
497
498
499
500
501
502
503
504
505
506
507
508
509
510
511
512
513
514
515
516
517
518
519
520
521
522
523
524
525
526
527
528
529
530
531
532
533
534
535
536
537
538
539
540
541
542
543
544
545
546
547
548
549
550
551
552
553
554
555
556
557
558
559
560
561
562
563
564
565
566
567
568
569
570
571
572
573
574
575
576
577
578
579
580
581
582
583
584
585
586
587
588
589
590
591
592
593
594
595
596
597
598
599
600
601
602
603
604
605
606
607
608
609
610
611
612
613
614
615
616
617
618
619
620
621
622
623
624
625
626
627
628
629
630
631
632
633
634
635
636
637
638
639
640
641
642
643
644
645
646
647
648
649
650
651
652
653
654
655
656
657
658
659
660
661
662
663
664
665
666
667
668
669
670
671
672
673
674
675
676
677
678
679
680
681
682
683
684
685
686
687
688
689
690
691
692
693
694
695
696
697
698
699
700
701
702
703
704
705
706
707
708
709
710
711
712
713
714
715
716
717
718
719
720
721
722
723
724
725
726
727
728
729
730
731
732
733
734
735
736
737
738
739
740
741
742
743
744
745
746
747
748
749
750
751
752
753
754
755
756
757
758
759
760
761
762
763
764
765
766
767
768
769
770
771
772
773
774
775
776
777
778
779
780
781
782
783
784
785
786
787
788
789
790
791
792
793
794
795
796
797
798
799
800
801
802
803
804
805
806
807
808
809
810
811
812
813
814
815
816
817
818
819
820
821
822
823
824
825
826
827
828
829
830
831
832
833
834
835
836
837
838
839
840
841
842
843
844
845
846
847
848
849
850
851
852
853
854
855
856
857
858
859
860
861
862
863
864
865
866
867
868
869
870
871
872
873
874
875
876
877
878
879
880
881
882
883
884
885
886
887
888
889
890
891
892
893
894
895
896
897
898
899
900
901
902
903
904
905
906
907
908
909
910
911
912
913
914
915
916
917
918
919
920
921
922
923
924
925
926
927
928
929
930
931
932
933
934
935
936
937
938
939
940
941
942
943
944
945
946
947
948
949
950
951
952
953
954
955
956
957
958
959
960
961
962
963
964
965
966
967
968
969
970
971
972
973
974
975
976
977
978
979
980
981
982
983
984
985
986
987
988
989
990
991
992
993
994
995
996
997
998
999
1000

1 reduction of contrast of the SMBGs, which arises due to a loss of mass/unit volume of
2 particles. After 120 h in SBF an extensive apatite phase had formed and the particles
3 greatly reduced in diameter (<150 nm), less than the mean diameter of the particles
4 before immersion (250 nm). Dissolution from the SMBG may therefore lead to a
5 supersaturation of Ca ions in the SBF solution and subsequent reprecipitation of Ca
6 and P rich crystals on their surface.
7
8
9

10
11
12 Although hMSC response to SiO₂ particles has been investigated previously, [19, 37,
13 38], the response of SMBGs with hMSCs has not. Therefore this was an aim of this
14 study. Unlike bulk materials, the biological response of small particles is highly
15 dependent on their size and their specific surface area [39, 40]. It is difficult to
16 compare with previous studies because of differences in the particle size and
17 composition and in the cell types investigated. The majority of studies with hMSCs
18 have used mesoporous silica sub-micron particles designed for drug delivery
19 applications. In these previous studies, no toxicity was observed when hMSCs were
20 exposed to hexagonal mesoporous silica (mean diameters of 110 -160 nm) of various
21 concentrations (0-200 µgml⁻¹) for different exposure times (10 min – 1 h), although
22 the cells were only monitored for 24 h after exposure [19, 37, 38]. Several studies on
23 dense silica (calcium-free) particles are based on targeting cancer cells. Viability of
24 human lung (bronchial alveolar cell line) cells decreased when exposed to 50 µgml⁻¹
25 silica nanoparticles (mean size of 46 nm) for 24 h [41]. A reduction in viability was
26 also seen in HeLa cells (a commonly used immortalised human cell line derived from
27 cervical cancer) exposed to silica particles (mean diameter of 200 nm) for 4 h [42].
28
29
30
31
32
33
34
35
36
37
38
39
40
41
42
43

44 Cell function is controlled through numerous intracellular signalling events which can
45 be triggered or altered by the uptake of the particles [38]. Uptake by endocytosis is
46 greatly influenced by the physical properties of the particles including their surface
47 charge, size and shape of the particles [38, 40, 43]. A common feature of all the cells
48 in the previous studies was that uptake of the particles was observed. The spherical
49 particles used in the current study were slightly larger than those used previously, so it
50 was important to observe whether the particles were taken up by the hMSCs and to
51 assess whether the particles caused any toxicity.
52
53
54
55
56
57
58
59
60
61
62
63
64
65

1
2
3
4
5
6
7
8
9
10
11
12
13
14
15
16
17
18
19
20
21
22
23
24
25
26
27
28
29
30
31
32
33
34
35
36
37
38
39
40
41
42
43
44
45
46
47
48
49
50
51
52
53
54
55
56
57
58
59
60
61
62
63
64
65

In the current study, cells were exposed to three concentrations of SMBGs for 24 h (a pulse) and the particles were removed as the media was changed. The cell behaviour was then monitored in culture (chase) and compared to cells that had not been exposed to particles.

Some spherical SMBGs (mean surface area $28 \text{ m}^2\text{g}^{-1}$ and diameter of 250 nm) appeared to have been internalised by hMSCs in endosomes via the non-specific cellular uptake of endocytosis (Fig. 6). Notably a few individual SMBGs appeared to localise inside the cell cytoplasm, suggesting that they may have escaped the endosomal pathway (Fig. 7). This is a similar uptake route to what was observed previously with mesoporous silica particles [38].

Several of the SMBGs appeared to dissolve inside the hMSCs (Fig 7). The particles appeared to reduce in density in their centre, in some cases forming hollow spheres. Calcium containing SMBGs are expected to be more prone to dissolution than silica particles in aqueous environments because calcium disrupts the silica network, reducing its network connectivity (mean number of bridging -Si-O-Si- bonds per silicon atom) and therefore its stability in solution [10]. The hollowing out of spherical bioactive glass microparticles (300-355 μm) has previously been observed extracellularly [44]. Intracellular dissolution of the particles would mean increased soluble silica and calcium ion content within the cell. Changes in intracellular calcium are essential regulators of many physiological processes including oxidative stress and cell death. During overload of the intracellular calcium mitochondria maintain calcium homeostasis by orchestrating a diverse range of cellular activities and ultimately cell death [45, 46]. Therefore the decrease in cell metabolic activity observed (MTT, Fig. 4b) after 7 days of culture for the higher concentrations of $150 \mu\text{gml}^{-1}$ and $200 \mu\text{gml}^{-1}$ could be attributed to the mechanism of calcium homeostasis by the mitochondria. In addition, this decrease in metabolic activity could not be interpreted as decreased proliferation (increased cell death) since it does not correlate with the amount of total DNA at day 7 (Fig. 4c), which indicates that none of the SMBG concentrations significantly reduced cell number.

In addition, some SMBGs were also observed to remain in the extracellular environment (not removed by the media changes and washes), which could contribute

1 to the decrease in metabolic activity. The particles would also dissolve as function of
2 time, releasing soluble silica and calcium ions. Previous studies that administered
3 bioactive glass dissolution products to human osteoblasts [46] and that cultured
4 osteoblasts on 70S30C (70 mol% SiO₂, 30 mol% CaO) scaffolds [7] showed that the
5 dissolution products caused a decrease in metabolic activity, which correlated to
6 enhanced extracellular matrix deposition. Also, The LIVE/DEAD (Supplementary
7 Fig. 3) and LDH assays (Fig. 4a) indicated that the SMBGs did not cause significant
8 levels of cytotoxicity.
9

10
11
12
13
14
15
16 It would be important to establish whether the effect on cell proliferation is the result
17 of position and trafficking of SMBG inside the cell, therefore, further and more
18 thorough uptake studies are essential as they will provide insight into the SMBG
19 interactions with the cells and consequently allowing their most appropriate use for
20 bone tissue regeneration applications.
21
22
23
24
25

26 27 **5 Conclusion**

28
29 Spherical bioactive glass particles with a mean diameter of 250 nm were successfully
30 produced with an optimised sol-gel processing route. The combination of cell viability
31 assays and imaging techniques was critical in understanding SMBG interactions with
32 mesenchymal stem cells. We successfully showed that SMBG were internalised into
33 hMSCs resulting in partial dissolution of the SMBGs. The viability assays confirmed
34 that none of the SMBG concentrations tested here induced any major cytotoxicity
35 when exposed to hMSCs and were only seen to reduce cell metabolism at higher
36 doses of 150 and 200 µgml⁻¹. The study shows that SMBG are potential candidates for
37 applications in regenerative medicine.
38
39
40
41
42
43
44
45

46 47 **Acknowledgements**

48
49 Dr Mahmoud Ardakani is thanked for his assistance with TEM imaging. The EPSRC
50 (departmental studentship and EP/E057098/1) and the Royal Academy of Engineering
51 are thanked for funding.
52
53
54
55
56
57
58
59
60
61
62
63
64
65

1
2
3
4
5
6
7
8
9
10
11
12
13
14
15
16
17
18
19
20
21
22
23
24
25
26
27
28
29
30
31
32
33
34
35
36
37
38
39
40
41
42
43
44
45
46
47
48
49
50
51
52
53
54
55
56
57
58
59
60
61
62
63
64
65

References

1. Hench LL, Polak JM. Third-Generation Biomedical Materials. *Science* 2002; 295(5557): p. 1014-1017.
2. Hench LL, Splinter R, Allen W, Greenlee JT. Bonding mechanism at the interface of ceramic prosthetic materials. *J Biomed Mater Res* 1972;2(1): p. 117-41.
3. Pereira MM, Clark AE, Hench LL. Effect of texture on the rate of hydroxyapatite formation on gel-silica surface. *J Am Ceram Soc* 1995;78(9): p. 2463-8.
4. Hong Z, Reis RL, Mano JF. Preparation and in vitro characterization of novel bioactive glass ceramic nanoparticles. *J Biomed Mater Res* 2008; 88A(2): p. 304-313
5. Jones JR, Hench LL. Effect of surfactant concentration and composition on the structure and properties of sol-gel-derived bioactive glass foam scaffolds for tissue engineering. *J Mater Sci.* 2003; 38(18): p. 3783-3790.
6. Saravanapavan P, Jones JR, Pryce RS, Hench LL., Bioactivity of gel- glass powders in the CaO-SiO₂ system:A comparison with ternary (CaO-P₂O₅-SiO₂) and quaternary glasses (SiO₂-CaO-P₂O₅-Na₂O). *J Biomed Mater Res* 2002. 66A: p. 110-119.
7. Jones JR, Tsigkou O, Coates EE, Stevens MM, Polak JM, Hench LL. Extracellular matrix formation and mineralization on a phosphate-free porous bioactive glass scaffold using primary human osteoblast (HOB) cells. *J Biomater* 2007; 28(9): p. 1653-1663.
8. Ebisawa Y, Kokubo T, Ohura K, Yamamuro T. Bioactivity of SiO₂-CaO based glasses: In vitro evaluation. *J Mater Sci - Mater Med* 1990; 1: p. 239-244.
9. Martinez A, Izquierdo-Barba I, Vallet-Regi M. Bioactivity of a CaO-SiO₂ Binary Glasses System. *Chem Mater* 2000;12(10): p. 3080-3088.
10. Lin S, Ionescu C, Pike K, Smith M., Jones JR. Nanostructure evolution and calcium distribution in sol-gel derived bioactive glass. *J Mater Chem* 2009;19: p. 1276 - 1282.
11. Green DL, Lin JS, Lam YF, Hu MZC, Schaefer DW, Harris MT. Size, volume fraction, and nucleation of Stober silica nanoparticles. *J. Colloid Interface Sci.* 2003;266(2): p. 346-358.
12. Zhao Y, Zou J, Shi W, Tang L. Preparation and characterization of mesoporous silica spheres with bimodal pore structure from silica/hyperbranched polyester nanocomposites. *Microporous Mesoporous Mater* 2006; 92(1-3): p. 251-258.
13. Zhao Y, Zou J, Shi W. In situ synthesis and characterization of lead sulfide nanocrystallites in the modified hyperbranched polyester by gamma-ray irradiation. *Mater Sci Eng B* 2005;121(1-2): p. 20-24.
14. Jones JR, Ehrenfried LM, Hench LL. Optimising bioactive glass scaffolds for bone tissue engineering. *Biomaterials* 2005; 27(7): p. 964-973.
15. Christensen KA, Myers JT, Swanson JA. pH-dependent regulation of lysosomal calcium in macrophages. *J Cell Sci* 2002; 115(3): p. 599-607.
16. Peters K, Unger RE, Kirkpatrick CJ. Effects of nano-scaled particles on endothelial cell function in vitro: Studies on viability, proliferation and inflammation. *J Mater Sci- Mater Med* 2004; 15: p. 319-323.

17. Motskin M, Wright DM, Muller K, Kyle N, Gard TG, Porter AE., Skepper, J.N. Hydroxyapatite nano and microparticles: Correlation of particle properties with cytotoxicity and biostability. *Biomaterials* 2009; 30(19): p. 3307-3317.
18. Porter AE, Müller K, Skepper J, Midgley P, Welland M., Uptake of C60 by human monocyte macrophages, its localization and implications for toxicity: Studied by high resolution electron microscopy and electron tomography. *Acta Biomaterials* 2006;2(4): p. 409-419.
19. Huang DM, Chung TH, Hung Y, Lu F, Wu SH, Mou CY, Yao M, Chen YC. Internalization of mesoporous silica nanoparticles induces transient but not sufficient osteogenic signals in human mesenchymal stem cells. *Toxicol Appl Pharmacol* 2008;231(2): p. 208-215.
20. Lin YS, Tsai CP, Huang HY, Kuo CT, Hung Y, Huang DM, Chen YC, Mou CY. Well-ordered mesoporous silica nanoparticles as cell markers. *Chem Mater* 2005; 17: p. 4570-4573.
21. Park MZ, Annema W, Salvati A, Lesniak A, Elsaesser A, Barnes C, McKerr G, Howard CV, Lynch I, Dawson KA, Piersma AH, de Jong WH. In vitro developmental toxicity test detects inhibition of stem cell differentiation by silica nanoparticles. *Toxicol Appl Pharmacol* 2009; 240: 108-116.
22. Pittenger MF, Mackay AM, Beck SC, Jaiswal RK, Douglas R, Mosca JD, Moorman MA, Simonetti DW, Craig S, Marshak R. Multilineage potential of adult human mesenchymal stem cells. *Science* 1999; 284 (5411): p. 143-147.
23. Amaral M, Costa MA, Lopes MA, Silva RF, Santos JD, Fernandes MH. Si3N4-bioglass composites stimulate the proliferation of MG63 osteoblast-like cells and support the osteogenic differentiation of human bone marrow cells. *Biomaterials* 2002; 23(24): p. 4897-4906.
24. Katayama M, Battista W-M, Kao A, Hidalgo A, Peired AJ, Thomas SA, Frenette PS. Signals from the sympathetic nervous system regulate hematopoietic stem cell egress from bone marrow. *Cell* 2006; 124 (2): p. 407-421.
25. Saravanapavan, P., Hench, L.L., Mesoporous calcium silicate glasses. II. Textural characterisation. *J Non-Cryst Solids* 2003; 318(1-2): p. 14-26.
26. Coleman NJ, Hench LL. A gel-derived mesoporous silica reference material for surface analysis by gas sorption 1. Textural features. *Ceram Int* 2000; 26(2): p. 171-178.
27. Kokubo T, Kushitani H, Sakka S, Kitsugi T, Yamamuro T. Solutions able to reproduce in vivo surface-structure changes in bioactive glass-ceramic A-W. *J Biomed Mater Res* 1990; 24: p. 721-734.
28. Porter AE, Patel N, Skepper JN, Best SM, Bonfield W. Comparison of in vivo dissolution processes in hydroxyapatite and silicon-substituted hydroxyapatite bioceramics. *Biomaterials* 2003; 24(25): p. 4609-4620.
29. Porter AE, Best SM, Bonfield W. Ultrastructural comparison of hydroxyapatite and silicon-substituted hydroxyapatite for biomedical applications. *J Biomed Mater Res A* 2004; 68A(1): p. 133-141.
30. Lu CW, Hung Y, Hsiao JK, Yao M, Chung TH, Lin YS, Wu SH, Hsu SC, Liu HM, Mou CY, Yang CS, Huang DM, Chen YC. Bifunctional Magnetic Silica Nanoparticles for Highly Efficient Human Stem Cell Labeling. *Nano Lett.* 2006; 7(1): p. 149-154.
31. Richet P, Mysen BO, Ingrin J. High-temperature X-ray diffraction and Raman spectroscopy of diopside and pseudowollastonite. *Phys Chem Miner* 1998; 25(6): p. 401-14.

- 1 32. Sing SW, Everett DH, Haul AW, Moscou L, Pierotti RA, Rouquerol J,
2 Siemieniowska T. Reporting physisorption data for a Gas/Solid systems. *Pure*
3 *Appl Chem* 1985; 57: p. 603-619.
- 4 33. Stöber W, Fink A, Bohn E. Controlled growth of monodisperse silica spheres
5 in the micron size range. *J Colloid Interface Sci* 1968; 26(1): p. 62-69.
- 6 34. Skipper LJ, Sowrey FE, Pickup DM, Drake KO, Smith ME. Saravanapavan P,
7 Hench LL. Newport RJ. The structure of a bioactive calcia-silica sol-gel glass.
8 *J Mater Chem* 2005; 15(24): p. 2369-2374.
- 9 35. Xynos I, Edgar A, Buttery L, Hench LL. Gene-expression profiling of human
10 osteoblasts following treatment with the ionic products of Bioglass 45S5
11 dissolution. *J Biomed Mater Res* 2001; 55: p. 151-157.
- 12 36. Sepulveda P, Jones JR, Hench LL. Characterization of melt-derived 45S5 and
13 sol-gel-derived 58S bioactive glasses. *J Biomed Mater Res* 2001; 58(6): p.
14 734-740.
- 15 37. Huang DM, Hung Y, Ko BS, Hsu SC, Chen WH, Chien CL, Tsai CP, Kuo C,
16 Kang JC, Yang CS, Mou CY, Chen YC. Highly efficient cellular labeling of
17 mesoporous nanoparticles in human mesenchymal stem cells: implication for
18 stem cell tracking. *FASEB J* 2005; 19: p. 2014-2016.
- 19 38. Huang X, Teng X, Chen D, Tang F, He J. The effect of the shape of
20 mesoporous silica nanoparticles on cellular uptake and cell function.
21 *Biomaterials* 2009; 31(3): p. 438-448.
- 22 39. Yuan Y, Liu C, Qian J, Wang J, Zhang Y. Size-mediated cytotoxicity and
23 apoptosis of hydroxyapatite nanoparticles in human hepatoma HepG2 cells.
24 *Biomaterials* 2010; 31 (4): p. 730-740.
- 25 40. Chung TH, Wu SH, Yao M, Lu CW, Lin YS, Hung Y, Mou CY, Chen YC,
26 Huang DM. The effect of surface charge on the uptake and biological function
27 of mesoporous silica nanoparticles in 3T3-L1 cells and human mesenchymal
28 stem cells. *Biomaterials* 2007; 28(19): p. 2959-2966.
- 29 41. Lin WS, Huang YW, Zhou XD, Ma YF. In vitro toxicity of silica nanoparticles
30 in human lung cancer cells. *Toxicol Appl Pharmacol* 2006; 217(3): p. 252-
31 259 .
- 32 42. Gratton SEA, Ropp PA, Pohlhaus PD, Luft JC, Madden VJ, Napier ME, and
33 DeSimone JM. The effect of particle design on cellular internalization
34 pathway. *Proc Nat Acad Sci* 2008; 105(33) p. 11613-11618.
- 35 43. Chithrani BD, Ghazani AA, Chan W. Determining the Size and Shape
36 Dependence of Gold Nanoparticle Uptake into Mammalian Cells. *Nano Lett*
37 2006; 6(4): p. 662-668.
- 38 44. Radin S, Ducheyne P, Falaize S, Hammond A. In vitro transformation of
39 bioactive glass granules into Ca-P shells. *J Biomed Mater Res* 2000; 49(2): p.
40 264-272.
- 41 45. Szabadkai G, Duchen MR. Mitochondria: The Hub of Cellular Ca²⁺ Signaling.
42 *Physiology* 2008; 23(2): p. 84-94.
- 43 46. Bootman MD, Collins TJ, Peppiatt CM, Prothero LS, MacKenzie L, De Smet,
44 P, Travers M, Tovey SC, Seo JT, Berridge MJ, Ciccolini F, Lipp P. Calcium
45 signalling--an overview. *Seminars in Cell & Developmental Biology* 2001;
46 12(1): p. 3-10.
- 47 47. Tsigkou O, Jones JR, Polak JM, Stevens MM. Differentiation of fetal
48 osteoblasts and formation of mineralized bone nodules by 45S5 Bioglass®
49 conditioned medium in the absence of osteogenic supplements. *Biomaterials*
50 2009; 30(21): p. 3542-3550.

Figure caption:

Figure 1: XRD spectra of BGPs as a function of calcination temperatures of 680, 700 and 800°C. W indicates a peak corresponding to the presence of a crystalline wollastonite phase

Figure 2: a) TEM micrograph of the optimised BGPs. b) EDX analysis of a BGP showing Si, O and Ca peaks.

Figure 3: TEM micrographs of BGP exposed to SBF for a-b) 48h showing dissolution of the particles and nucleation of a finer particulate phase on their surface. c) 120 h exposure to SBF showing more widespread nucleated deposits on the surface of the BGPs. SAED pattern obtained from the cluster of particles. d) EDX analysis of BGPs after immersion in SBF for 120h.

Figure 5: Confocal 3-D imaging of a live hMSCs incubated without BGPs b) with 100µg/ml of BGP for 24 h at 37 °C. c-d) 3D reconstructions from boxed region in (b). The particles were internalised inside the cell and associated with the actin fibres of the cell. (Red= actin fibres, blue = nucleus and green = BGP);

Figure 4: Cytotoxicity assays. Cell viability was monitored using: LDH release, b) metabolic activity (MTT), and c) total DNA of hMSCs after a 24 h pulse of BGPs followed by 4 and 7 days chase. Values represent the mean ± SD of two individual experiments each performed in quadruplicate. (* $p < 0.05$ relative to control, without BGP).

Figure 6: TEM micrographs of hMSC following incubation a) without BGPs (post-stained) b-c) with 100 µg/ml of BGPs for 24 h. b) Particles internalised inside a cell. c) Clusters of BGPs were encapsulated inside endosomes (region i) and individual BGPs were present inside the cell cytoplasm (ii) (post-stained section), (N: the nucleus, NM: the nuclear membrane, ER: the endoplasmic reticulum, C: the cytoplasm).

Figure 7: TEM micrographs of hMSCs exposed to 100 µg/ml of BGPs after 24 h exposure (post-stained). a) A hollow nanoparticle adjacent to the nuclear membrane (region iii). Particles around the endosomal membrane (region iv), b) EDX analysis of region iii, showing peaks of Si and Ca and c) region iv showing peaks of Ca.

Supplementary Figure 1: FTIR spectra of BGP before (BG-H20) and after calcination at 680°C

Supplementary Figure 2: Nitrogen adsorption/desorption isotherm for the P3 sample (sintered at 680°C).

Supplementary Figure 3: Fluorescent Microscopy of LIVE/DEAD cytotoxicity assay. hMSC a) without BGNPs b) 100µg/ml and c) 200µg/ml of BGNPs after 24h incubation at 37 °C. The figure shows the cell population with the cytoplasm of the live cells stained with the Calcein AM (green) and the nucleus of the dead cells stained with EthD-1 (red).

Figure 1
[Click here to download high resolution image](#)

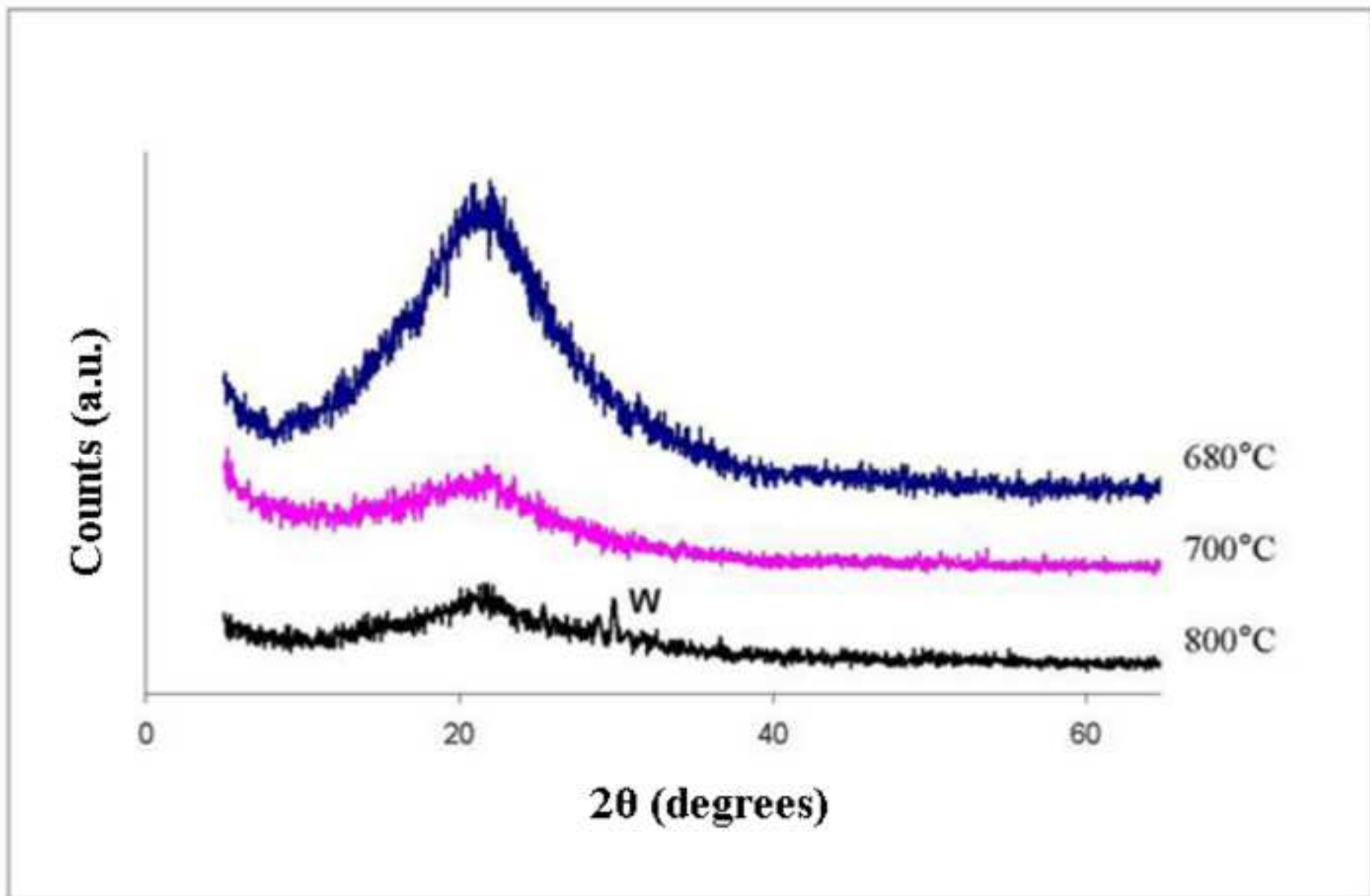


Figure 2
[Click here to download high resolution image](#)

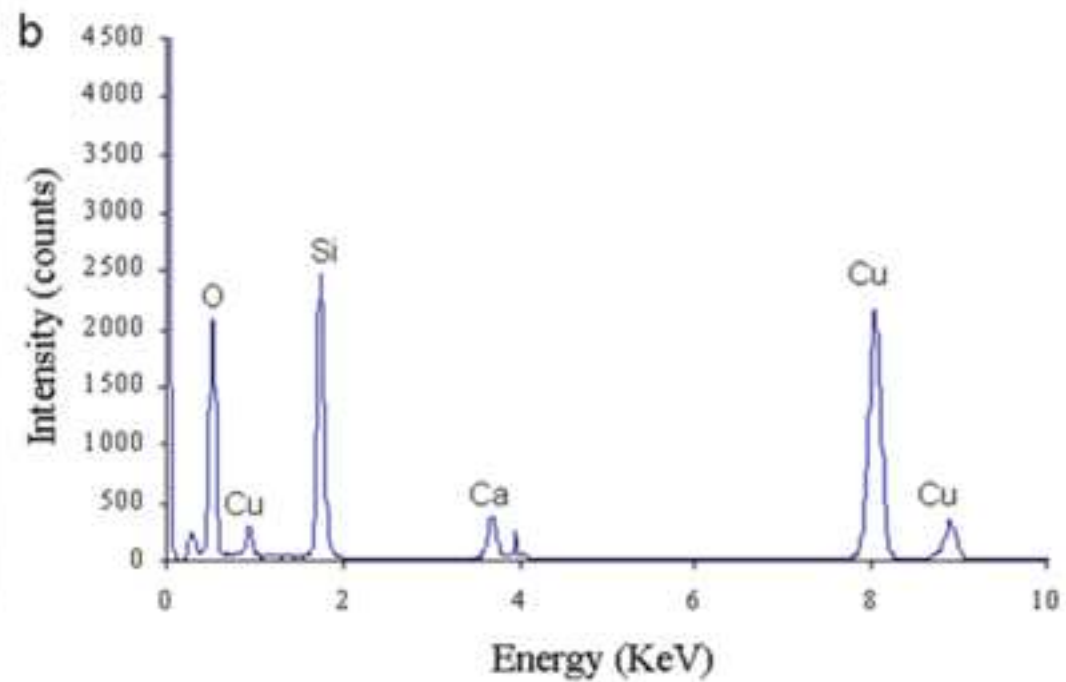
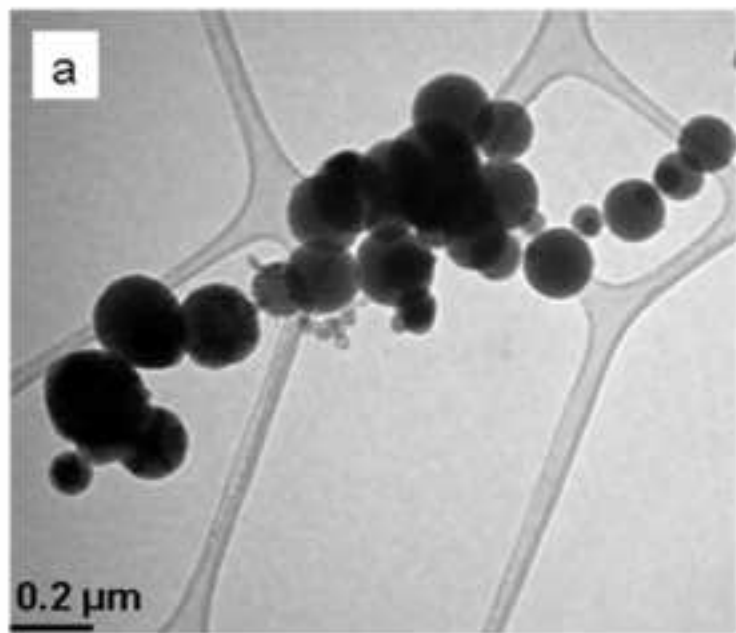


Figure 3
[Click here to download high resolution image](#)

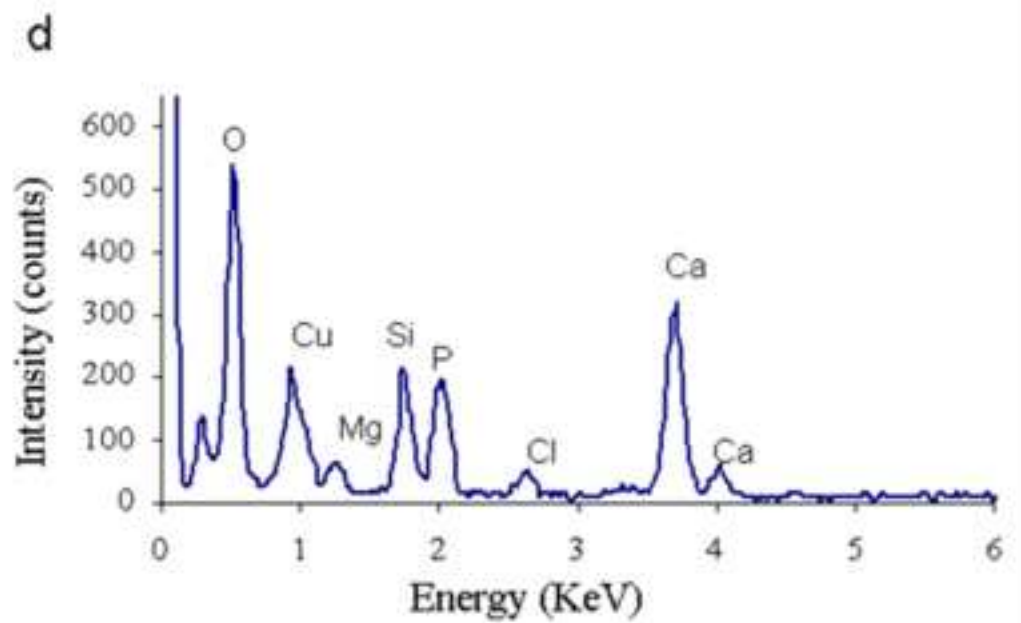
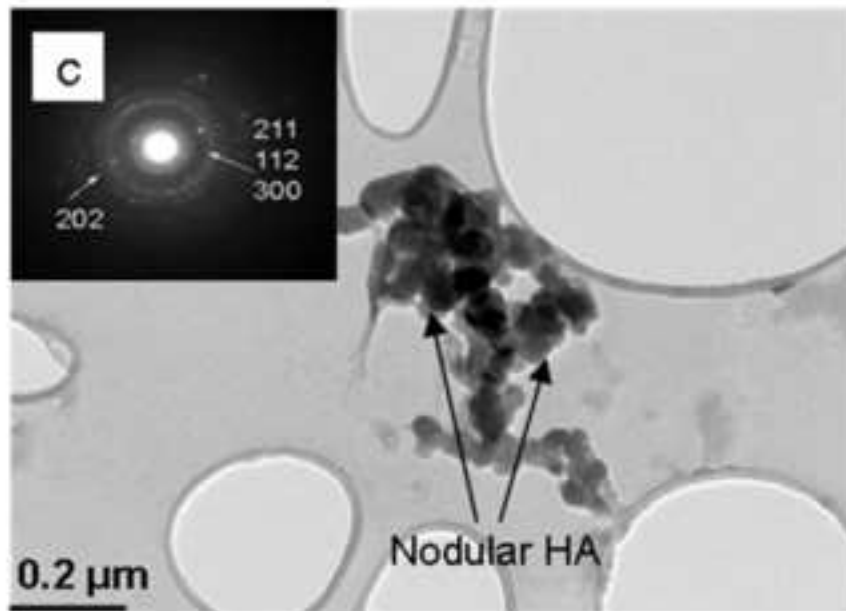
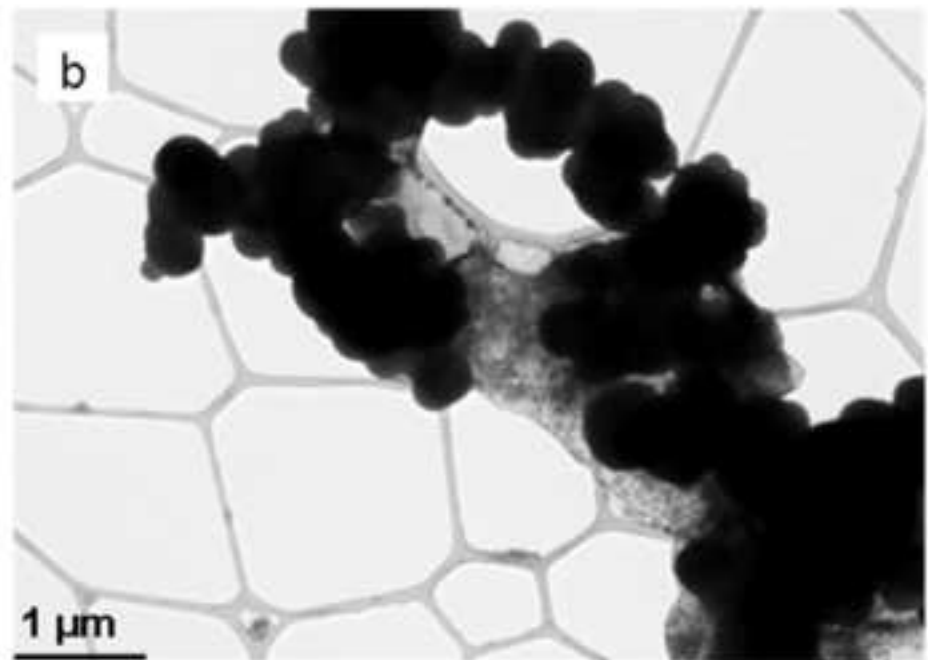
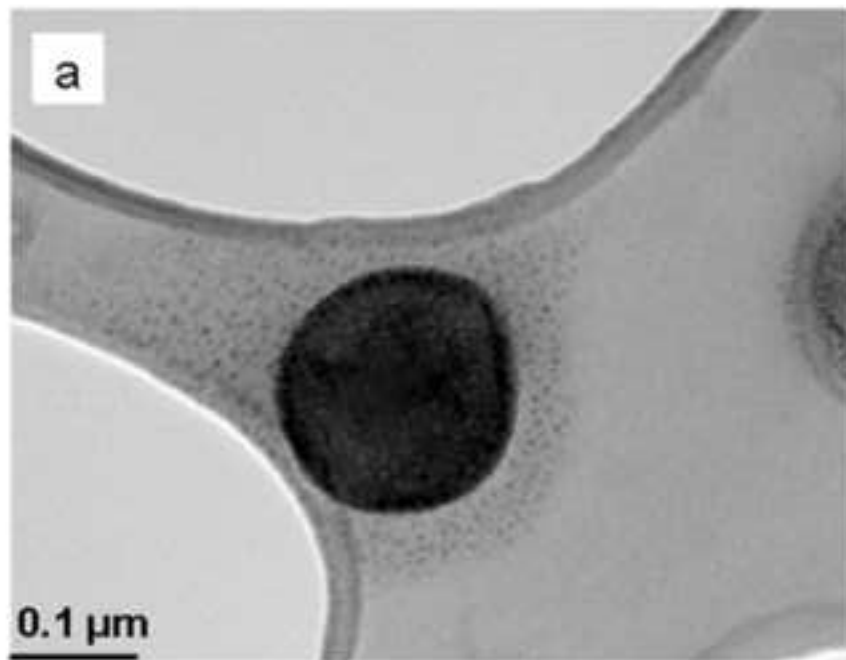


Figure 4
[Click here to download high resolution image](#)

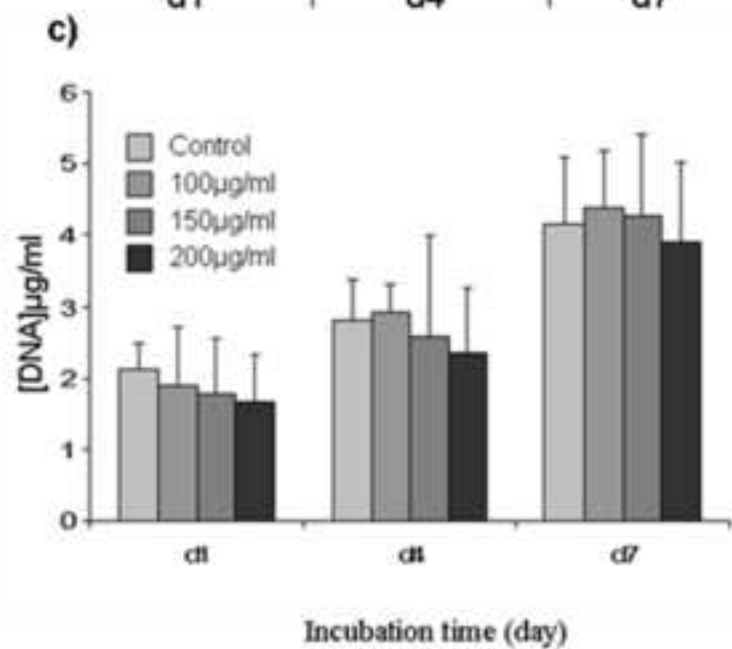
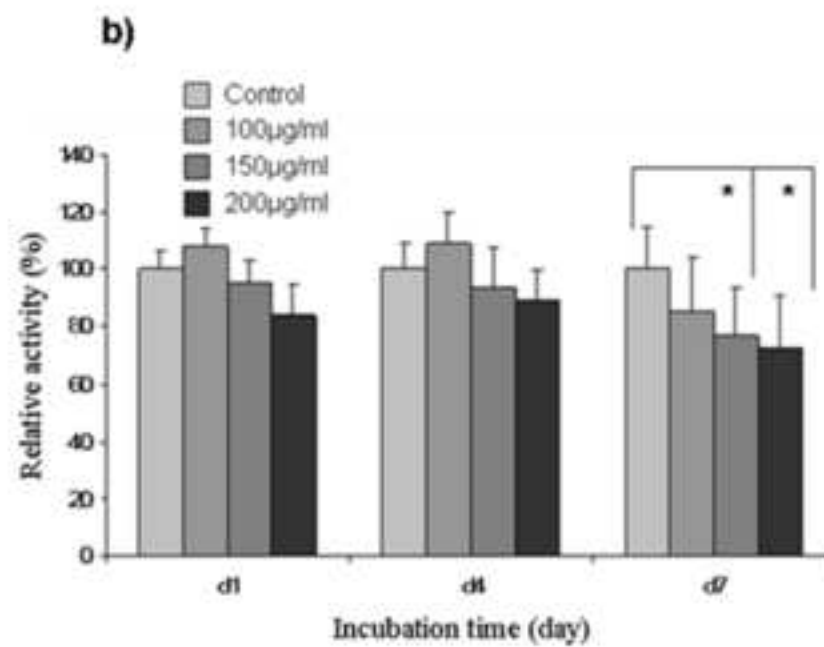
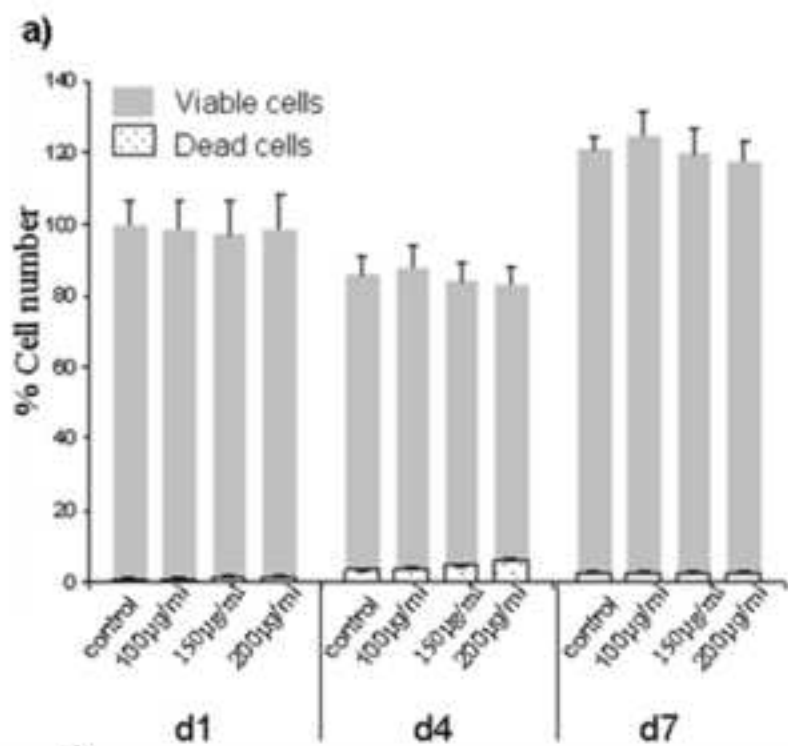


Figure 5
[Click here to download high resolution image](#)

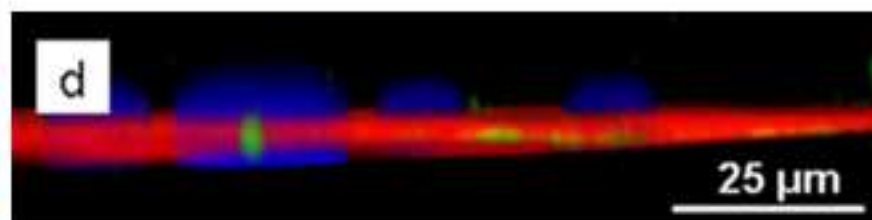
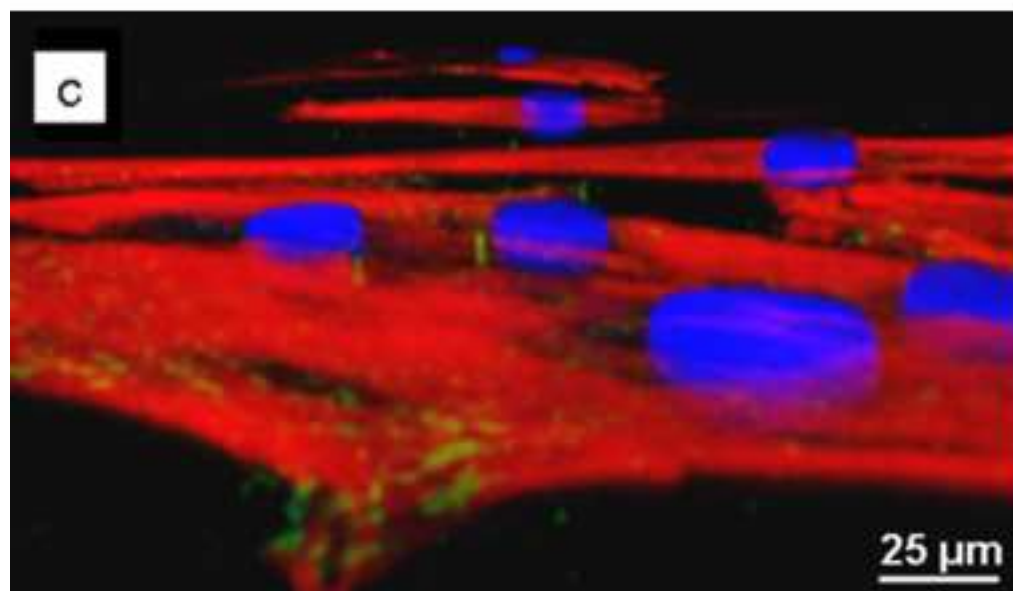
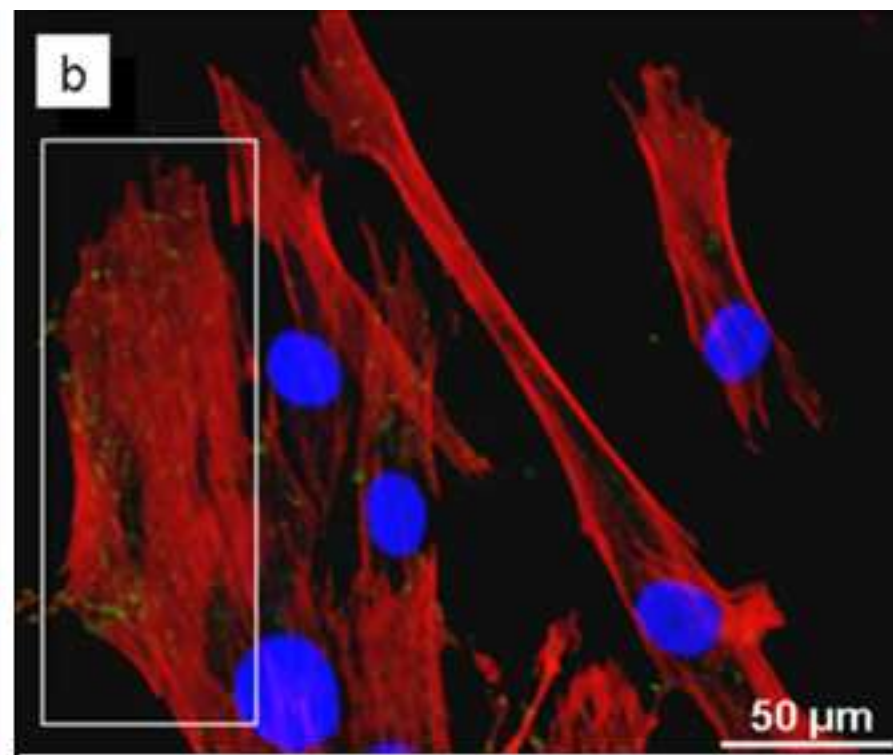
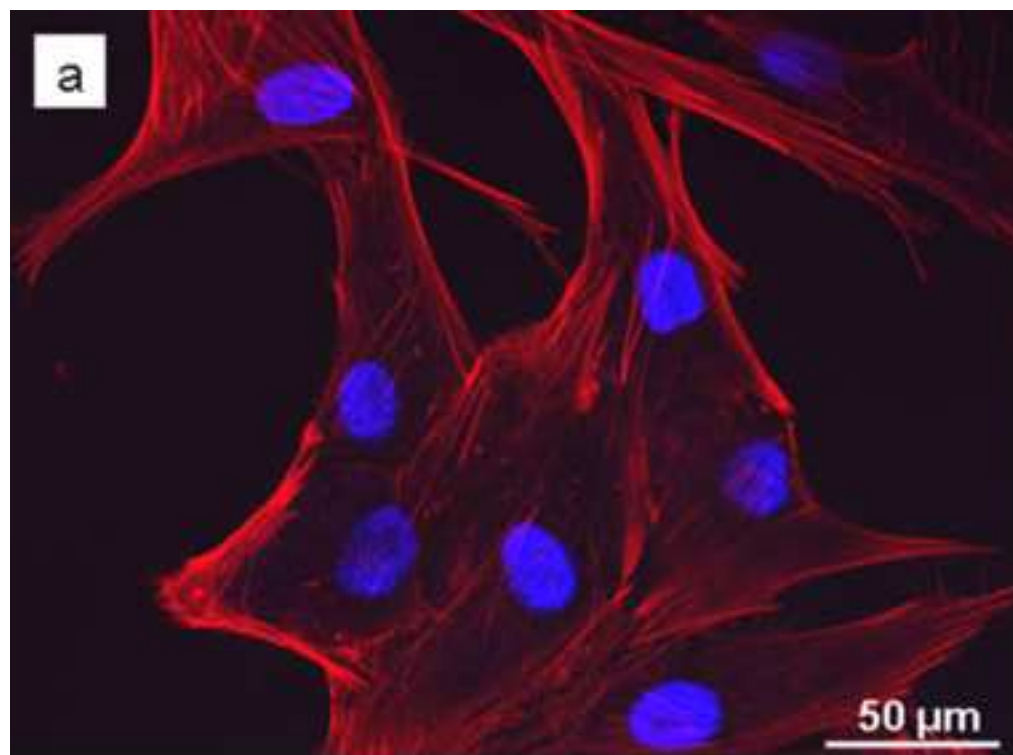


Figure 6
[Click here to download high resolution image](#)

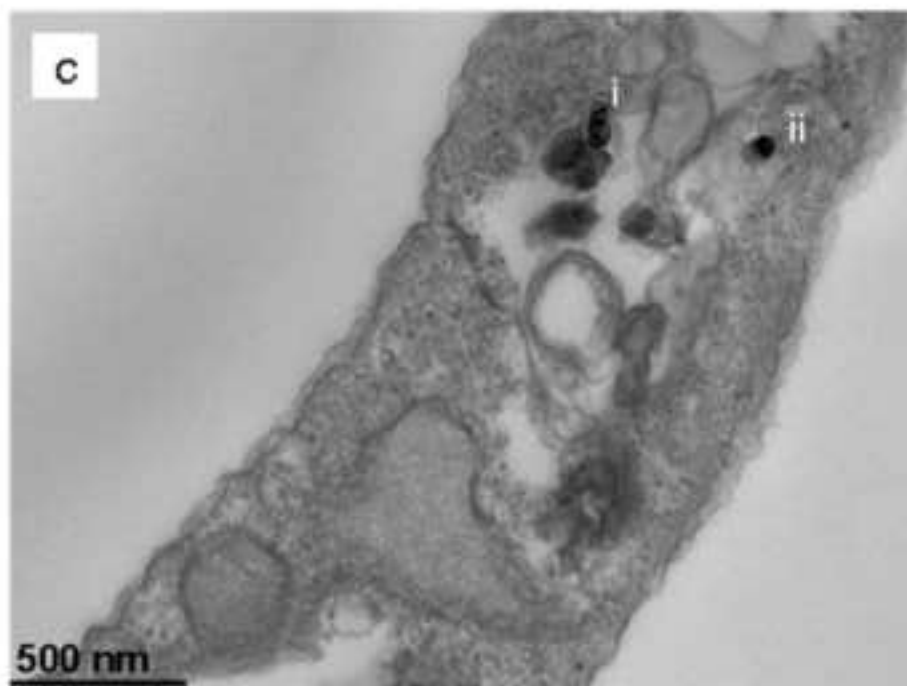
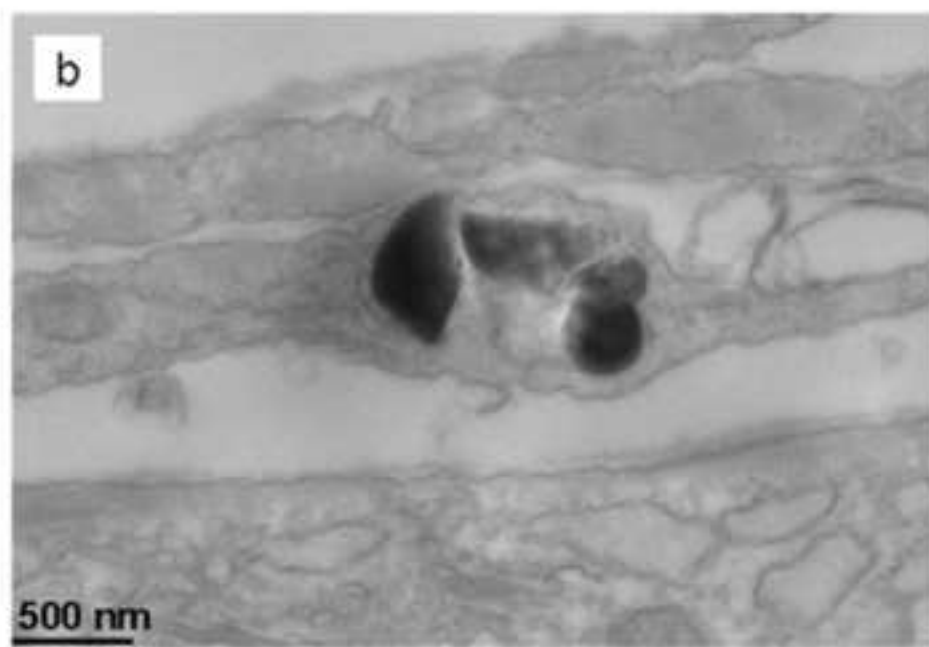
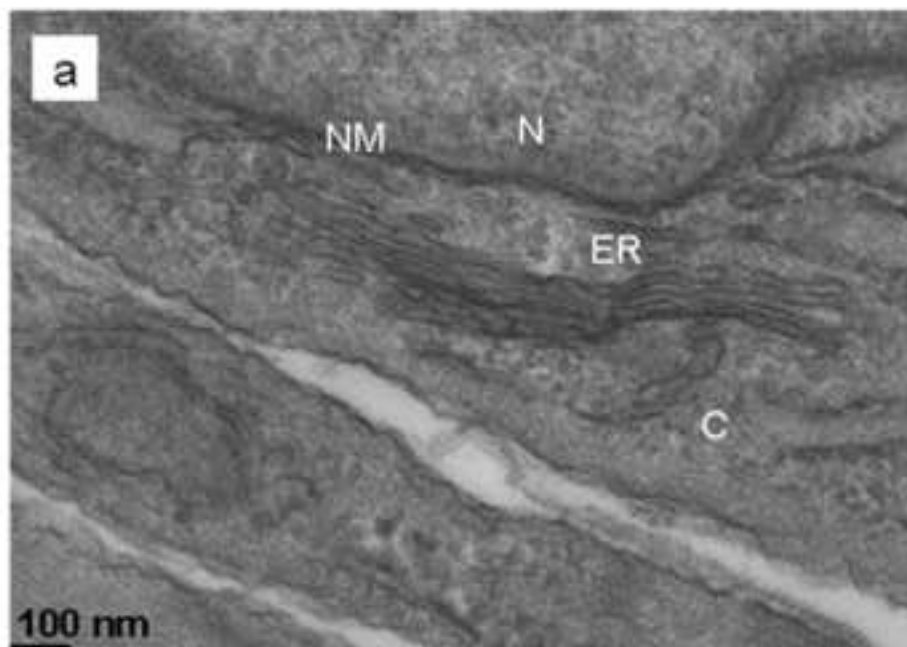
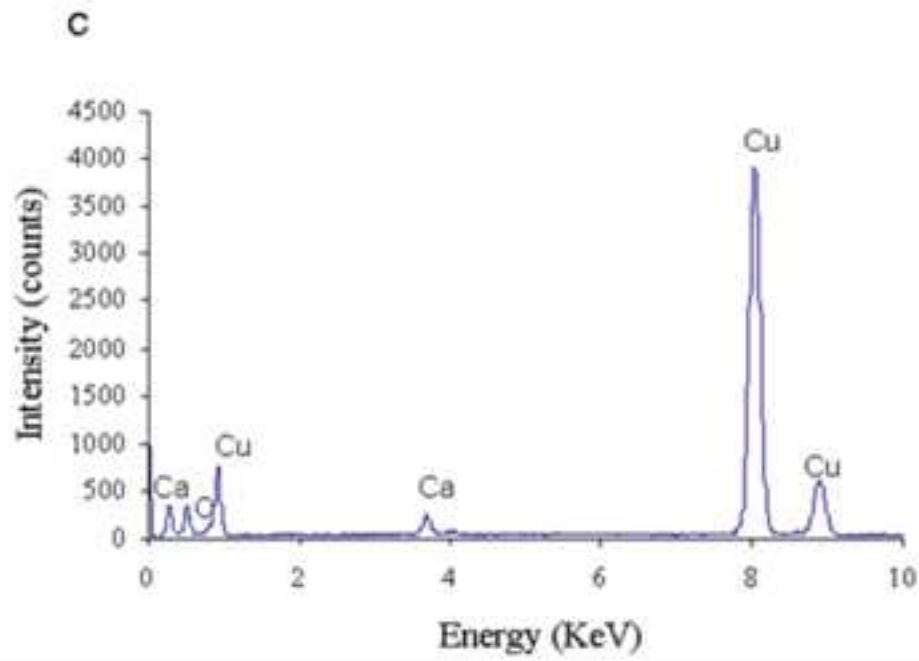
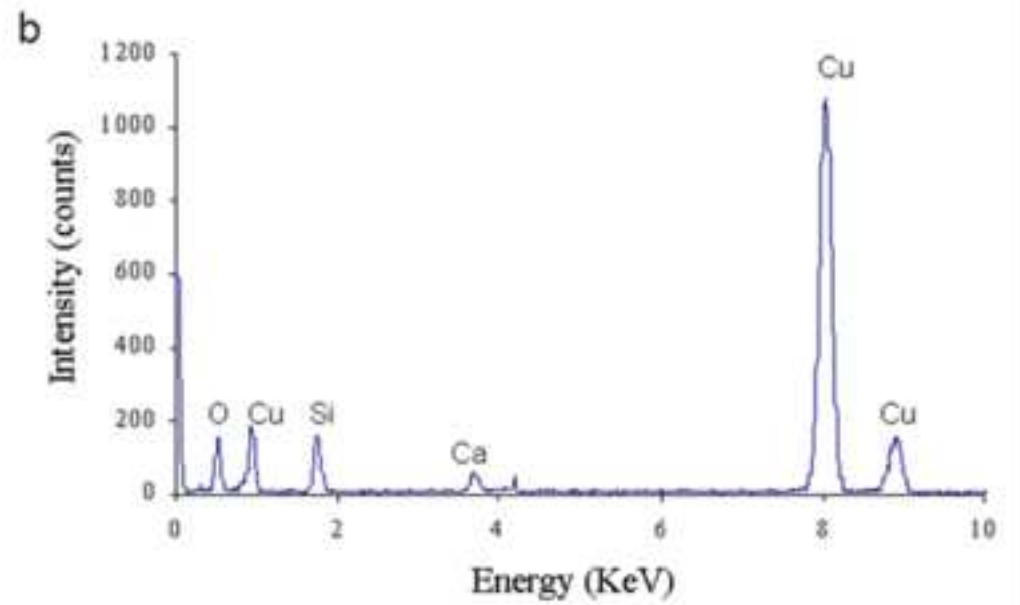
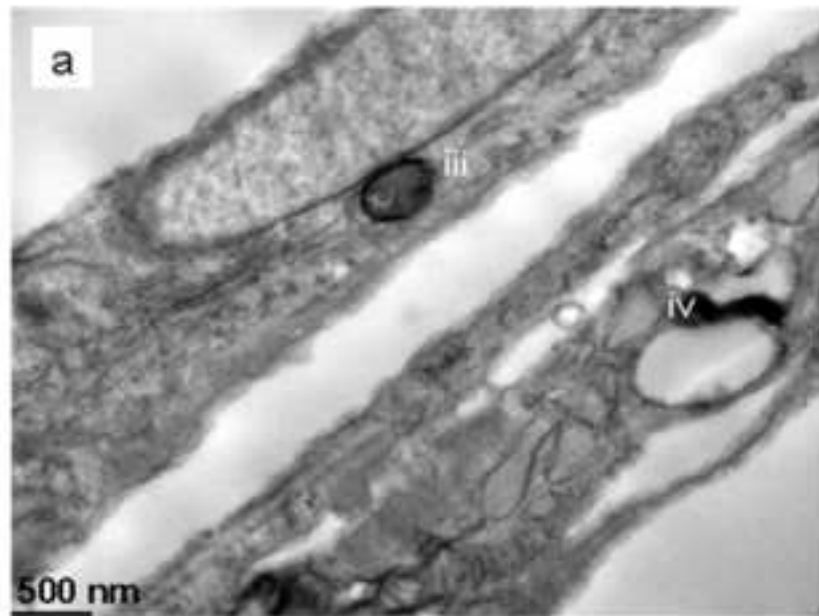


Figure 7
[Click here to download high resolution image](#)



Movie/Animation

[Click here to download Movie/Animation: labbaf movie.avi](#)

